Supplementary Information for

Shortening the intramolecular Pd-Pd distance for photoactive dinuclear Pd(II) complexes

*Weixue Fan†, Hua-Chao Liu†, Yi Zhang, Qizheng Zhang, Xiaoyu Guo, Jingsheng Miao Chuluo Yang and Kai Li**

College of Materials Science and Engineering, Shenzhen University, 1066 Xueyuan Blvd., Shenzhen 518055

Email: kaili@szu.edu.cn

General information

Unless otherwise indicated, all starting materials were obtained from commercial suppliers and were used without further purification. All the reaction solvents were purified by solvent purification system prior to use.

The ^{1}H and ^{13}C nuclear magnetic resonance (NMR) spectra were recorded in deuterated chloroform ($CDCl_3$) solution on Bruker NMR spectrometer with tetramethylsilane (TMS, δ 0.00) as the internal standard. High-resolution electrospray (EI) mass spectra were performed on SCIEX TripleTOF6600 nanoLCMS. Thermogravimetric analysis (TGA) was undertaken using a PerkinElmer Instruments (Pyris1 TGA) at a heating rate of 10 °C/ min from 30 to 800 °C under a nitrogen flow environment. UV-vis absorption spectra were recorded on a Shimadzu UV-2700 recording spectrophotometer. Photoluminescence (PL) spectra were recorded on a Hitachi F-4600 fluorescence spectrophotometer. The lifetimes of fluorescence and delayed fluorescence were performed on PicoQuant Fluotime300. Absolute PLQYs were obtained using a Quantaurus-QY measurement system (C9920-02, Hamamatsu Photonics). Cyclic voltammetry (CV) was carried out in nitrogen-purged dichloromethane (oxidation scan) at room temperature with a CHI voltammetric analyzer. Tetrabutylammonium hexafluorophosphate ($TBAPF_6$) (0.1 M) was used as the supporting electrolyte. The conventional three-electrode configuration consists of a platinum working electrode, a platinum wire auxiliary electrode, and an Ag wire pseudo reference electrode with ferrocenium/ferrocene (Fc+ /Fc) as the internal standard.

Device Fabrication and Characterization

For devices fabrications, the layers of ITO/HATCN (5 nm)/TAPC (30 nm)/TCTA (15 nm)/DMIC-TRZ: 3% emitter (45 nm)/Na-An-BI (30-50 nm)/Liq (2 nm)/Al were successively deposited on the pre-cleaned ITO glass substrates at a pressure of less than 10^{-4} Pa. The ITO electrode with transmittance of over 90% in the visible region was used in fabricating the El devices. The ITO coated glass substrates with a sheet

resistance of 15 Ω square-1 were consecutively ultrasonicated with acetone/ethanol and dried with nitrogen gas flow, followed by 20 min ultraviolet light-ozone (UVO) treatment in a UV-ozone surface processor (PL16 series, Sen Lights Corporation). Then the sample was transferred to the deposition system. Both 8-hydroxyquinolinolato-lithium (Liq) as electron injection layer and aluminum (Al) as cathode layer were deposited by thermal evaporation at 5×10^{-5} Pa. Additionally, the organic layers were deposited at the rates of 0.2-3 Å/s. After the organic film deposition, Liq and Al layer were deposited with rates of 0.1 and 3 Å/s, respectively. The emitting area of the device is about 0.09 cm^2. The current density-voltage-luminance (*J-V-L*), L-EQE curves and electroluminescence spectra were measured using a Keithley 2400 source meter and an absolute EQE measurement system (C9920-12, Hamamatsu Photonics, Japan).

Synthesis of the materials

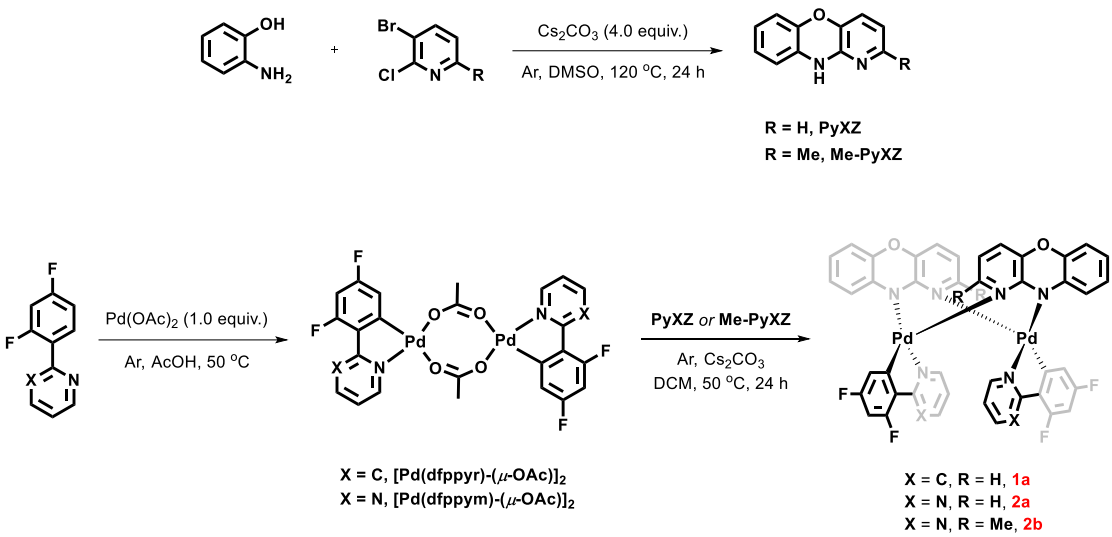

Scheme S1. Synthetic route of **1a**, **2a** and **2b**

10*H*-benzo[*b*]pyrido[2,3-*e*][1,4]oxazine (PyXZ): Under an argon atmosphere, to a 100 mL flask was added 3-bromo-2-chloropyridine (2.06 g, 10.00 mmol), 2-aminophenol (1.09 g, 10.00 mmol), Cs_2CO_3 (13.03 g, 40.00 mmol) and dry dimethyl sulfoxide (60 mL). The reaction mixture was stirred at 120 ℃ under argon atmosphere for 24 h. After cooling to room temperature, the reaction mixture was poured into 150

mL of water and extracted with EA (150 mL x 3). The combined organic phase was washed with brine (150 mL x 2), dried by anhydrous sodium sulfate and concentrated under vacuum, then purified by column chromatography on silica gel (eluent: CH_2Cl_2/EA = 10:1~7:1), providing the product **PyXZ** as a white solid. Yield: 48%. ^{1}H NMR (500 MHz, DMSO-d_6) δ (ppm): 8.99 (br s, 1H), 7.52 (dd, J_1 = 5.1, J_2 = 1.5 Hz, 1H), 6.88 (dd, J_1 = 7.7 Hz, J_2 = 1.4 Hz, 1H), 6.76 (td, J_1 = 7.2 Hz, J_2 =2.1 Hz, 1H), 6.69-6.52 (m, 4H).

2-methyl-10*H*-benzo[*b*]pyrido[2,3-*e*][1,4]oxazine (Me-PyXZ): The synthetic routes of **Me-PyXZ** is the same as that of **PyXZ**. The product **Me-PyXZ** was obtained as a white solid. Yield: 35%. ^{1}H NMR (500 MHz, DMSO-d_6) δ (ppm): 8.93 (br s, 1H), 6.68 (d, J = 7.8 Hz, 1H), 6.63-6.59 (m, 1H), 6.49 (d, J = 3.5 Hz, 2H), 6.44 (d, J = 7.7 Hz, 1H), 6.27 (d, J = 7.8 Hz, 1H), 2.03 (s, 3H).

Synthesis of 1a: Under an argon atmosphere, to a 100 mL flask was added 2-(2,4-difluorophenyl)pyridine (428.53 mg, 2.23 mmol) and $Pd(OAc)_2$ (500.00 mg, 2.23 mmol) and AcOH (30 mL). The reaction mixture was stirred at 50 ^{o}C under argon atmosphere overnight. After removing the solvent under reduced pressure, the residue was washed with diethyl ether to obtain product as a orange red solid. This dimer was used for the next step without any further purification. A mixture of the dimer (520.00 mg, 0.73 mmol), **PyXZ** (340.51 mg, 1.85 mmol), and Cs_2CO_3 (1.43 g, 4.38 mmol) in dichloromethane was stirred at 50 °C for 24 h in an argon atmosphere. After cooling to room temperature, the solvent was removed under vacuo and the crude product was purified by column chromatography on silica gel (eluent: petroleum ether/ethyl acetate = 4:1, *v/v*). The product **1a** was obtained as an orange red solid. Yield: 22%. ^{1}H NMR (400 MHz, Chloroform-*d*) δ (ppm): 8.06-7.99 (m, 2H), 7.82 (dd, J_1 = 7.8, J_2 = 1.5 Hz, 2H), 7.60-7.47 (m, 4H), 7.41 (dd, J_1 = 6.0, J_2 = 1.5 Hz, 2H), 6.56-6.50 (m, 4H), 6.48-6.30 (m, 6H), 6.25 (dd, J_1 = 7.4, J_2 = 1.5 Hz, 2H), 6.14 (dd, J_1 = 8.0, J_2 = 2.4 Hz, 2H), 5.92 (dd, J_1 = 7.4, J_2 = 6.0 Hz, 2H). HRMS (EI+) *m/z* calculated for $C_{44}H_{26}F_4N_6O_2Pd_2$: 960.0172, found: 960.0172. Anal. Calcd (%) for $C_{44}H_{26}F_4N_6O_2Pd_2$: C 55.08; H 2.73; N 8.76. Found: C 55.16; H 2.98; N 8.62.

Synthesis of 2a: The synthetic routes of **2a** is the same as that of **1a**. The product **2a** was obtained as an orange red solid. Yield: 20%. ^{1}H NMR (500 MHz, Chloroform-*d*) δ (ppm): 8.63 (dd, J_1 = 4.8, J_2 = 2.4 Hz, 2H), 8.15 (dd, J_1 = 5.7, J_2 = 2.3 Hz, 2H), 7.74 (dd, J_1 = 7.8, J_2 = 1.5 Hz, 2H), 7.40 (dd, J_1 = 6.1, J_2 = 1.5 Hz, 2H), 6.58-6.51 (m, 4H), 6.47 (dd, J_1 = 5.7, J_2 = 1.8 Hz, 2H), 6.42 (dd, J_1 = 7.8, J_2 =1.6 Hz, 2H), 6.29 (dd, J_1 = 7.4, J_2 = 1.5 Hz, 2H), 6.17 (dd, J_1 = 7.7, J_2 = 2.3 Hz, 2H), 5.96 (dd, J_1 = 7.3, J_2 = 6.1 Hz, 2H). HRMS (EI+) *m/z* calculated for $C_{42}H_{24}F_4N_8O_2Pd_2$: 962.0032, found: 962.0073. Anal. Calcd. for $C_{42}H_{24}F_4N_8O_2Pd_2{\cdot}CH_2Cl_2$: C 49.35, H 2.50, N 10.71; found: C 49.82, H 2.41, N 10.34.

Synthesis of 2b: The synthetic routes of **2b** is the same as that of **1a**. The product **2b** was obtained as an orange red solid. Yield: 16%. ^{1}H NMR (500 MHz, Chloroform-*d*) δ (ppm): 8.74 (dd, J_1 = 4.8, J_2 = 2.3 Hz, 2H), 7.71 (dd, J_1 = 5.7, J_2 = 2.3 Hz, 2H), 7.44 (d, J = 7.4 Hz, 2H), 7.06 (t, J = 5.2 Hz, 2H), 6.48-6.40 (m, 4H), 6.37-6.31 (m, 4H), 6.25 (d, J = 7.4 Hz, 2H), 6.20 (dd, J_1 = 8.0, J_2 = 2.4 Hz, 2H), 5.95 (d, J = 7.6 Hz, 2H), 2.53 (s, 6H). HRMS (EI+) *m/z* calculated for $C_{42}H_{28}F_4N_8O_2Pd_2$: 990.0345, found: 990.0356. Anal. Calcd. for $C_{44}H_{28}F_4N_8O_2Pd_2{\cdot}H_2O$: C 52.45, H 3.00, N 11.12; found: C 52.81, H 2.76, N 10.73.

Table S1. The selected bonds in the dinuclear Pd(II) complexes.

Bond length (Å)					
1a		**2a**		**2b**	
Pd1-C_{22}	1.995	Pd1-C_{32}	1.987	Pd1-C_{30}	1.988
Pd1-N_1	2.036	Pd1-N_1	2.037	Pd1-N_1	2.149
Pd1-N_3	2.018	Pd1-N_4	2.134	Pd1-N_4	2.057
Pd1-N_5	2.144	Pd1-N_5	2.031	Pd1-N_5	2.036
Pd2-C_{23}	1.990	Pd2-C_{42}	1.987	Pd2-C_{40}	1.987
Pd2-N_2	2.146	Pd2-N_2	2.134	Pd2-N_2	2.050
Pd2-N_4	2.034	Pd2-N_3	2.024	Pd2-N_3	2.153
Pd2-N_6	2.045	Pd2-N_7	2.019	Pd2-N_7	2.025
Pd1-Pd2	2.790	Pd1-Pd2	2.795	Pd1-Pd	2.781

Table S2. Crystal data and structure refinement for complexes **1a**, **2a** and **2b**.

Identification code	1a	2a	2b
Empirical formula	$C_{44}H_{26}F_4N_6O_2Pd_2$	$C_{42}H_{24}F_4N_8O_2Pd_2$	$C_{44}H_{28}F_4N_8O_2Pd_2$
Formula weight	959.51	961.49	989.54
Temperature/K	100	170.00	170.00
Crystal system	triclinic	monoclinic	triclinic
Space group	P-1	C2/c	P-1
a/Å	10.4030(6)	20.7115(13)	10.9051(4)
b/Å	14.4561(9)	26.5389(17)	13.0260(4)
c/Å	15.3486(9)	22.1807(13)	16.5638(5)
α/°	66.517(2)	90	81.1420(10)
β/°	82.651(2)	106.922(2)	78.4620(10)
γ/°	71.201(2)	90	67.0620(10)
Volume/Å^3	2004.1(2)	11664.0(13)	2115.50(12)
Z	2	12	2
ρ_{calc}g/cm^3	1.590	1.643	1.553
μ/mm^{-1}	0.961	5.440	0.914
F (000)	952.0	5712.0	984.0
Crystal size/mm^3	0.08 × 0.04 × 0.02	0.3 × 0.05 × 0.04	0.2 × 0.16 × 0.13
Radiation	MoKα (λ= 0.71073)	GaKα (λ= 1.34139)	MoKα(λ=0.71073)
2Θ range for data collection/°	4.136 to 52.958	4.842 to 121.474	4.252 to 55.04
Index ranges	-26 ≤ h ≤ 26, -25 ≤ k ≤ 34, -28 ≤ l ≤ 28	-26 ≤ h ≤ 26, -25 ≤ k ≤ 34, -28 ≤ l ≤ 28	-14 ≤ h ≤ 14, -16 ≤ k ≤ 16, -21 ≤ l ≤ 21
Reflections collected	80219	80219	53876
Independent reflections	8245 [R_{int} = 0.0645, R_{sigma} = 0.0841]	13415 [R_{int} =0.0832, R_{sigma} = 0.0719]	9702 [R_{int} =0.0368, R_{sigma} = 0.0241]
Data/restraints/ parameters	8245/0/523	13415/0/784	9702/0/543
Goodness-of-fit on F^2	1.042	1.080	1.049

Identification code	1a	2a	2b
Final R indexes [I>=2σ (I)]	R_1 = 0.0536	R_1 = 0.0440, wR_2	R_1 = 0.026
	wR_2 = 0.1084	= 0.0948	wR_2 = 0.0575
Final R indexes [all data]	R_1 = 0.0948	R_1 = 0.0724,	R_1 = 0.0315
	wR_2 = 0.1271	wR_2 = 0.1044	wR_2 = 0.0600
Largest diff. peak/hole / e Å^{-3}	0.75/-0.77	0.46/-0.86	0.40/-0.52
CCDC No.	2471134	2471136	2471137

Table S3. The selected angles in the dinuclear Pd(II) complexes

Angel (°)					
1a		**2a**		**2b**	
ΣPd1	360	ΣPd1	360	ΣPd1	360
ΣPd2	360	ΣPd2	360	ΣPd2	360
C^N_1-Pd1-PyXZ_1 (dihedral angle)	86.14	C^N_1-Pd1-PyXZ_1 (dihedral angle)	80.62	C^N_1-Pd1-PyXZ_1 (dihedral angle)	83.27
C^N_1-Pd1-PyXZ_2 (dihedral angle)	81.14	C^N_1-Pd1-PyXZ_2 (dihedral angle)	89.74	C^N_1-Pd1-PyXZ_2 (dihedral angle)	86.57
C^N_1- C^N_2 (dihedral angle)	20.69	C^N_1- C^N_2 (dihedral angle)	18.56	C^N_1- C^N_2 (dihedral angle)	16.89

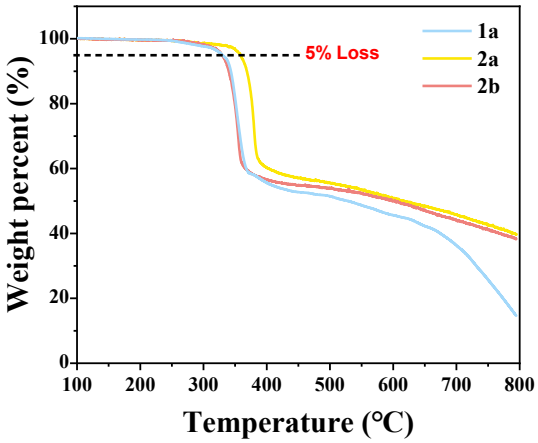

Figure S1. TGA curves of **1a**, **2a** and **2b**.

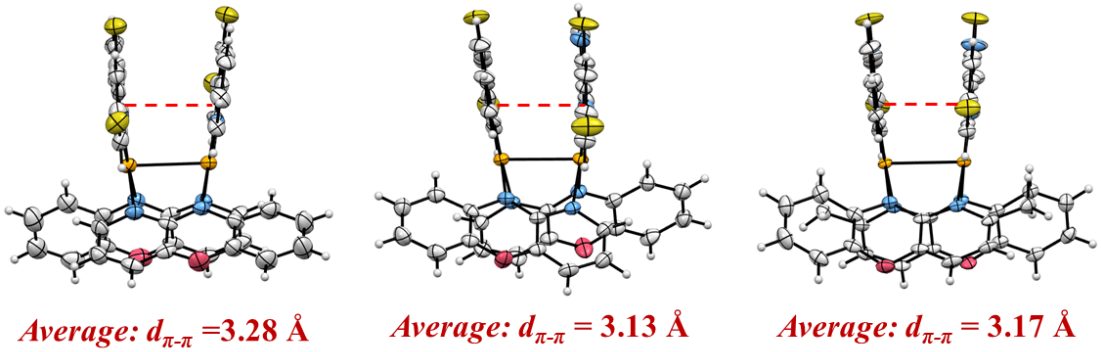

Figure S2. Intramolecular π-π interactions of **1a**, **2a** and **2b**.

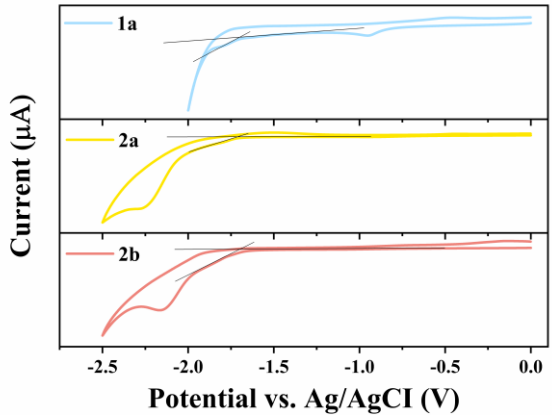

Figure S3. Cyclic voltammograms of **1a** (in DMF), **2a** and **2b** (in CH_3CN).

Table S4. Electrochemical data of the Pd(II) complexes.

Complexes	E_{pa} [a] (V)	E_{pc} [a] (V)	$E_{1/2(ox)}$ [a] (V)	E_{red} [a] (V)	E_{HOMO} [b] (eV)	E_{LUMO} [c] (eV)	E_g [d] (eV)
1a	0.50	0.42	0.46	-1.70	-4.73	-2.64	2.09
2a	0.54	0.46	0.50	-1.72	-4.77	-2.67	2.10
2b	0.48	0.40	0.44	-1.71	-4.71	-2.68	2.03

[a] Measured by cyclic voltammetry. [b] E_{HOMO} = -[($E_{1/2(ox)}$–0.53) + 4.8] eV, where 0.53 V denotes the $E(Cp_2Fe^{+/0})$ *vs.* Ag/AgCl and -4.8 eV is the energy level of ferrocene relative to the vacuum. [c] E_{LUMO} = -[(E_{red}–$E_{1/2}(Fc^+/Fc)$) + 4.8] eV, where $E_{1/2}(Fc^+/Fc)$ = 0.46 V in DMF for **1a** and $E_{1/2}(Fc^+/Fc)$ = 0.41 V in acetonitrile for **2a** and **2b**. [d] E_g = E_{LUMO}–E_{HOMO}.

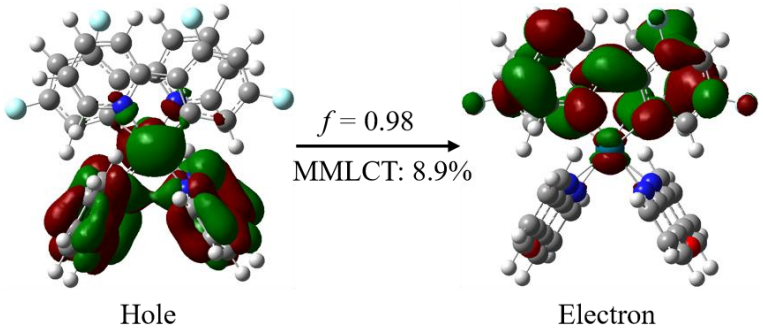

Figure S4. The natural transition orbitals (NTOs) representing the T_1 excited state of complex **1a**.

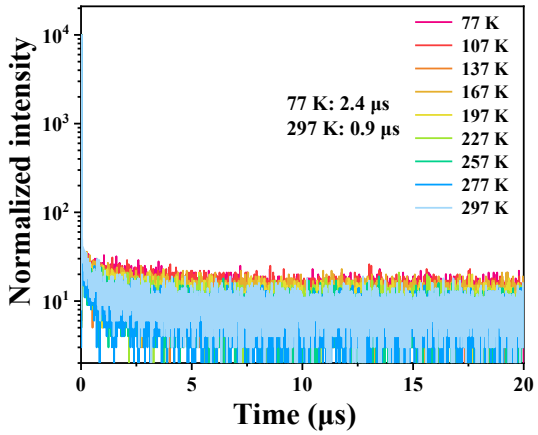

Figure S5. Variable-temperature PL decay characteristics of **1a** in PMMA film (10 wt.%).

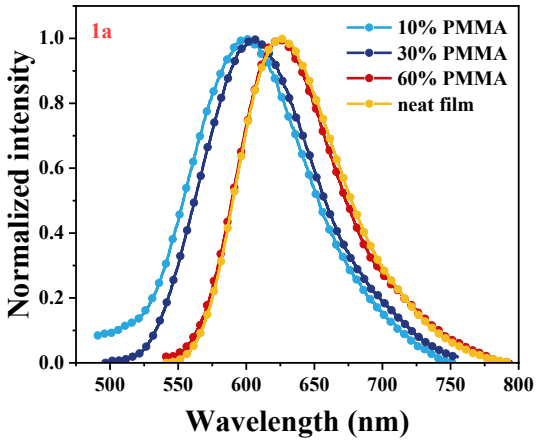

Figure S6. PL spectra of **1a** in PMMA at various concentration (10-60 wt.%) and neat films.

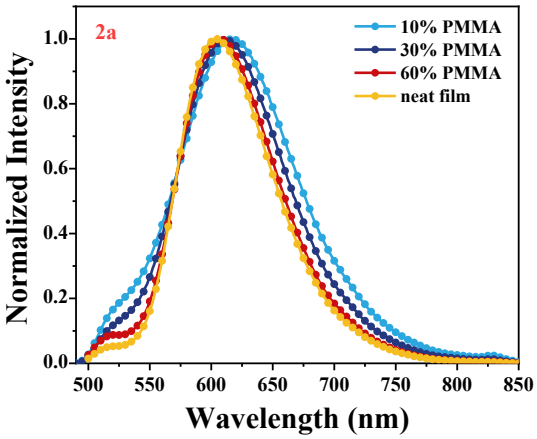

Figure S7. PL spectra of **2a** in PMMA at various concentration (10-60 wt.%) and neat films.

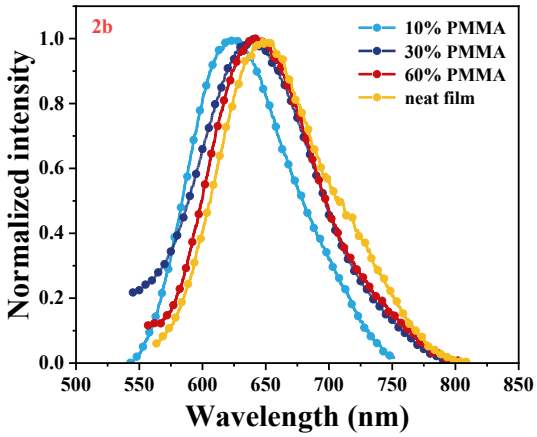

Figure S8. PL spectra of **2b** in PMMA at various concentration (10-60 wt.%) and neat films.

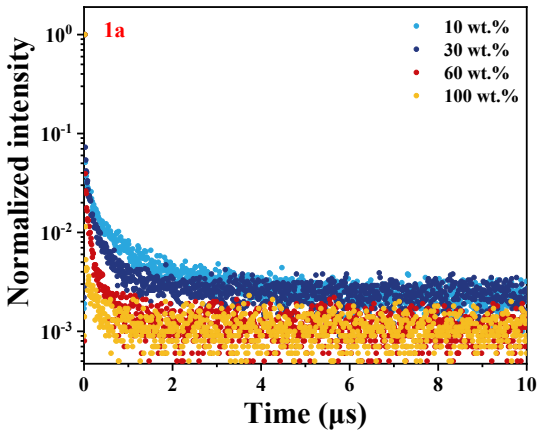

Figure S9. Variable-concentration PL decay characteristics of **1a** in PMMA film (10-100 wt.%).

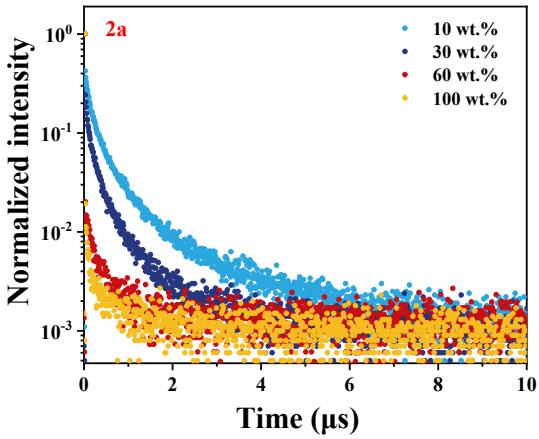

Figure S10. Variable-concentration PL decay characteristics of **2a** in PMMA film (10-100 wt.%).

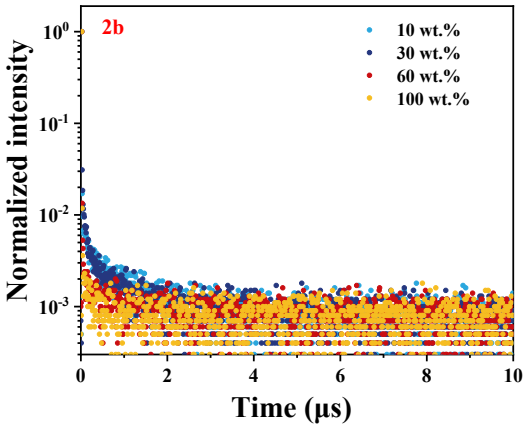

Figure S11. Variable-concentration PL decay characteristics of **2b** in PMMA film (10-100 wt.%).

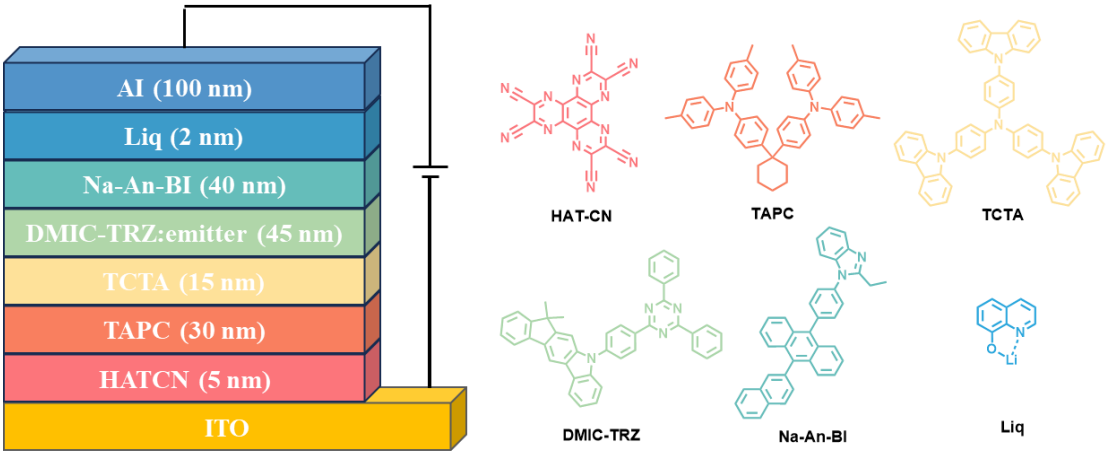

Figure S12. Device structure and molecular structures of selected functional materials.

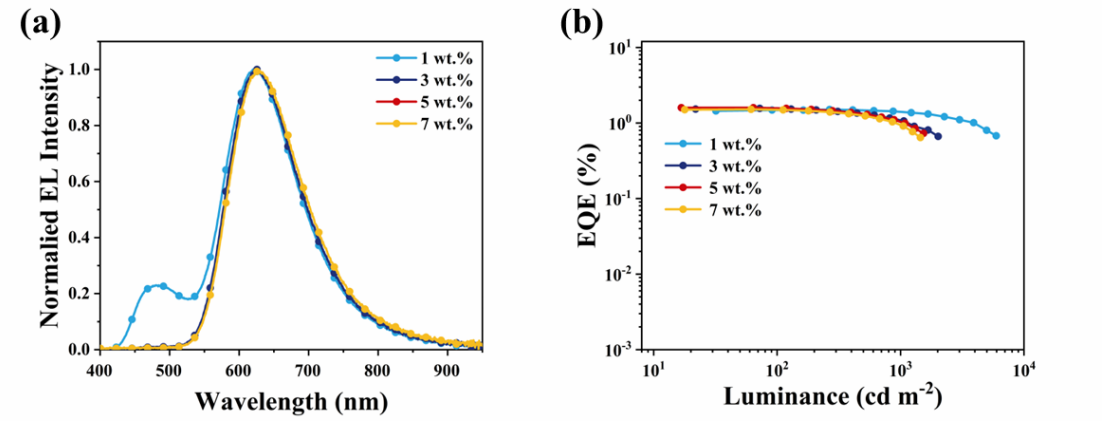

Figure S13. (**a**) Normalized EL spectra, and (**b**) EQE-luminance characteristics of OLEDs for various concentrations of complex **2a**.

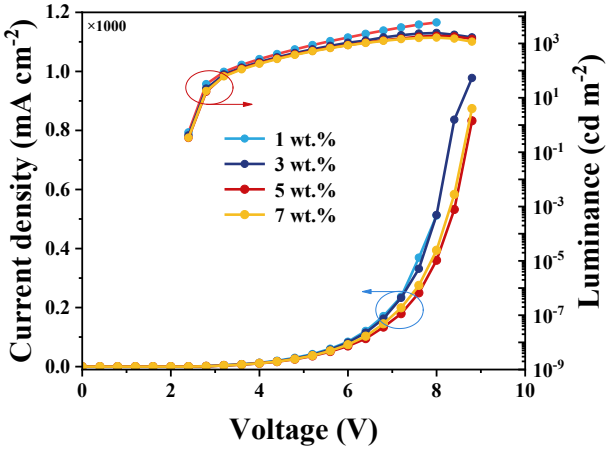

Figure S14. Current density-voltage-luminance (J-V-L) characteristics of OLEDs for various concentrations of complex **2a**.

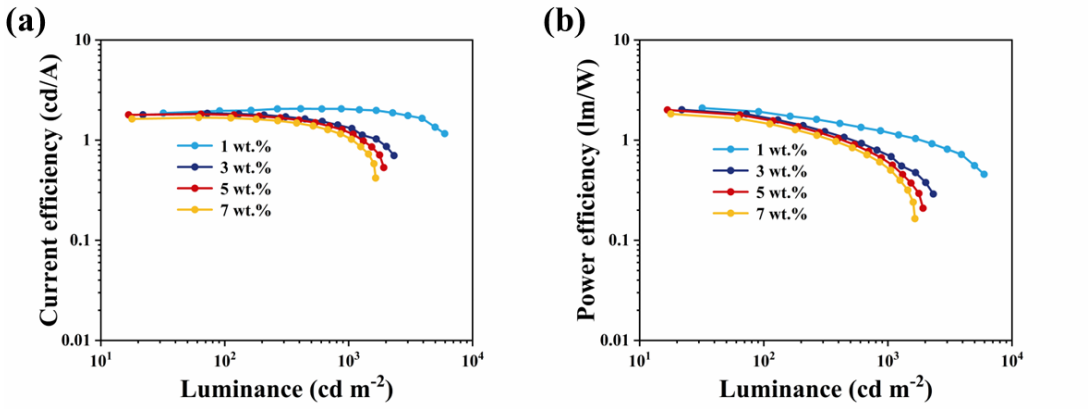

Figure S15. (**a**) Current density-voltage characteristics, and (**b**) luminance-voltage characteristics of OLEDs for various concentrations of complex **2a**.

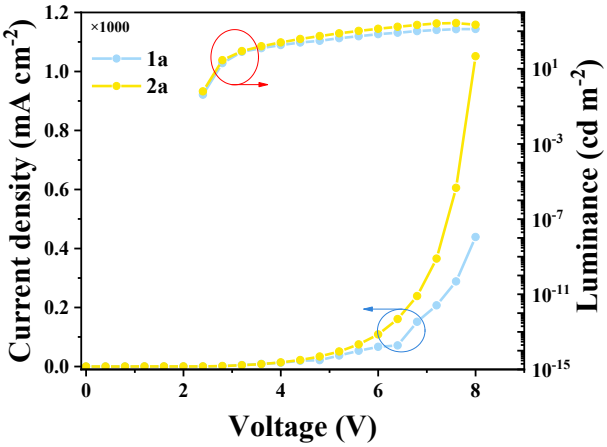

Figure S16. Current density-voltage-luminance (J-V-L) characteristics of OLEDs of Pd(II) complexes.

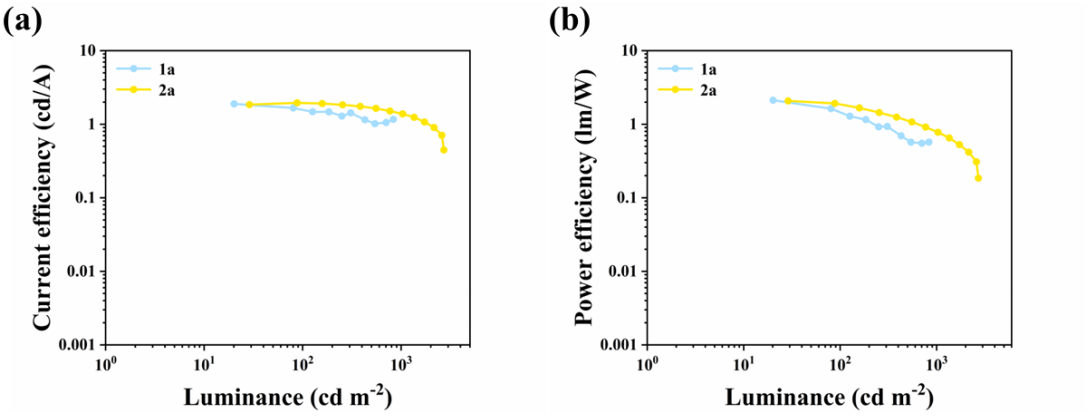

Figure S17. (**a**) Current density-voltage characteristics, and (**b**) luminance-voltage characteristics of OLEDs of Pd(II) complexes.

Table S5. Key performances of OLEDs based on **2a** as the emitter.

2a Concentration	***L*** **(cd m^{-2}) [a]**	**CE (cd A^{-1}) [b]**		**PE (lm W^{-1}) [c]**		**EQE (%) [d]**	
		Max.	**at 1000 cd m^{-2}**	**Max.**	**at 1000 cd m^{-2}**	**Max.**	**at 1000 cd m^{-2}**
1 wt.%	5952	2.1	2.0	2.1	1.2	1.5	1.4
3 wt.%	2440	1.8	1.4	2.0	0.7	1.6	1.1
5 wt.%	1918	1.8	1.2	2.0	0.6	1.6	1.0
7 wt.%	1649	1.7	1.0	1.8	0.5	1.5	0.9

[a] Maximum radiance. [b] Current efficiency. [c] Power efficiency. [d] External quantum efficiency.

Table S6. Key performances of OLEDs based on **1a** and **2a** (3 wt.%) as the emitters.

	L **(cd m^{-2}) [a]**	**CE (cd A^{-1}) [b] Max.**	**PE (lm W^{-1}) [c] Max.**	**EQE (%) [d] Max.**
1a	1309	1.9	2.1	1.1
2a	2440	1.8	2.0	1.6

[a] Maximum radiance. [b] Current efficiency. [c] Power efficiency. [d] External quantum efficiency.

^{1}H NMR and HR-MS spectroscopies

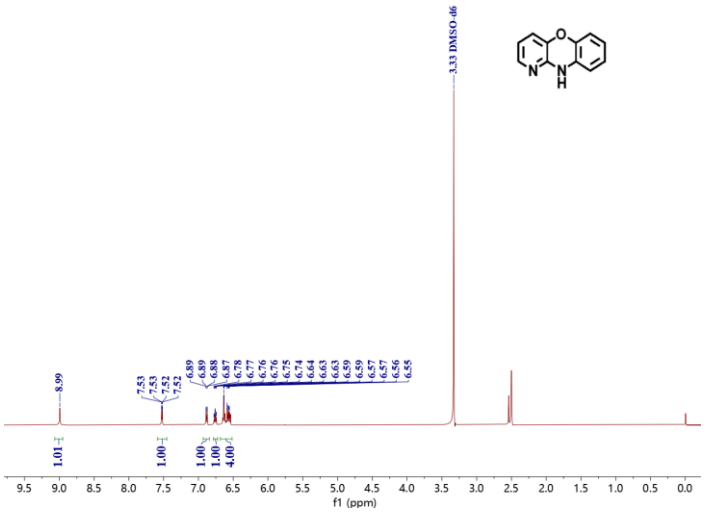

Figure S18. ^{1}H NMR spectrum of compound **PyXZ** in DMSO-*d*6.

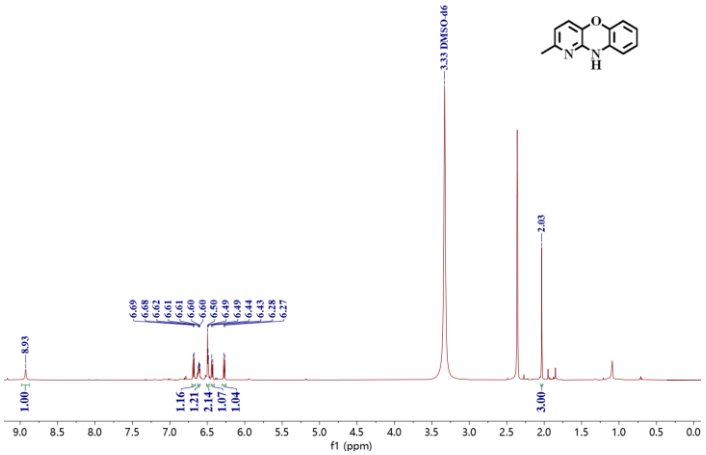

Figure S19. ^{1}H NMR spectrum of compound **Me-PyXZ** in DMSO-d_6.

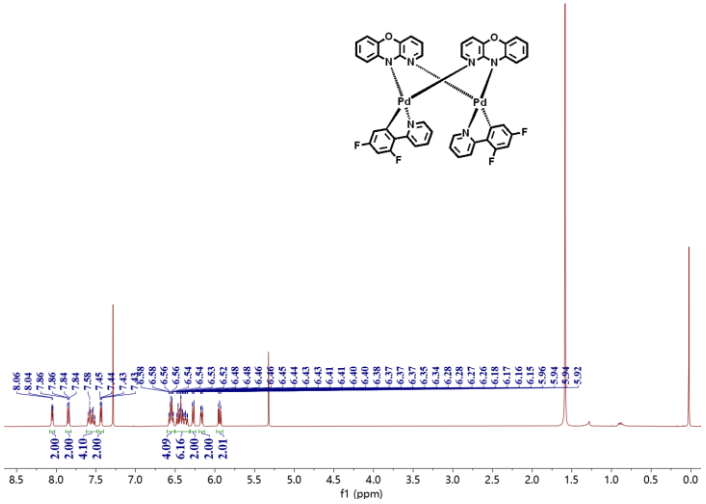

Figure S20. ^{1}H NMR spectrum of compound **1a** in $CDCl_3$.

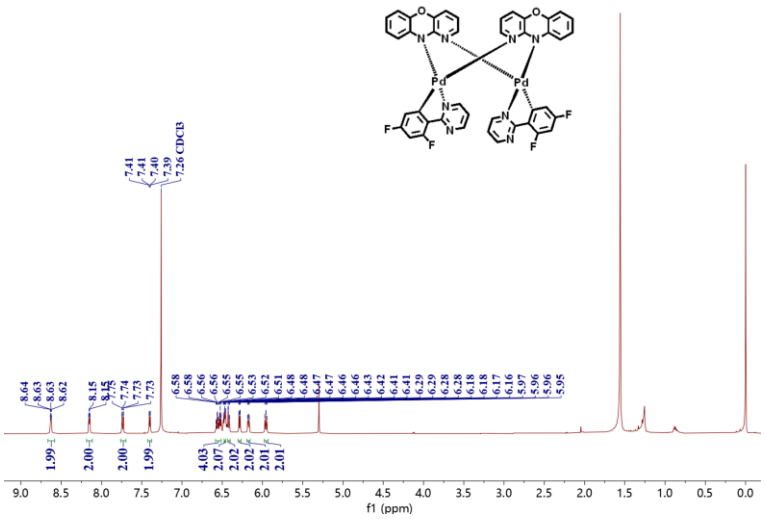

Figure S21. ^{1}H NMR spectrum of compound **2a** in $CDCl_3$.

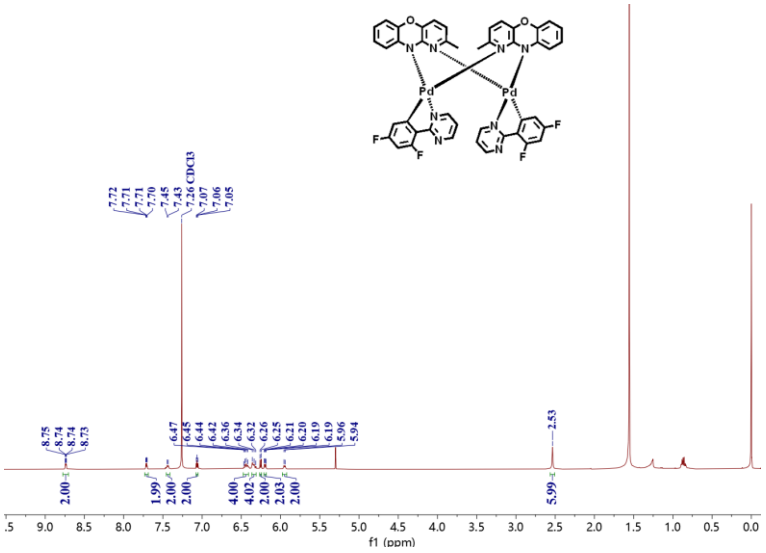

Figure S22. ^{1}H NMR spectrum of compound **2b** in $CDCl_3$.

HRMS (EI+)
m/z found

HRMS (EI+)
m/z calculated

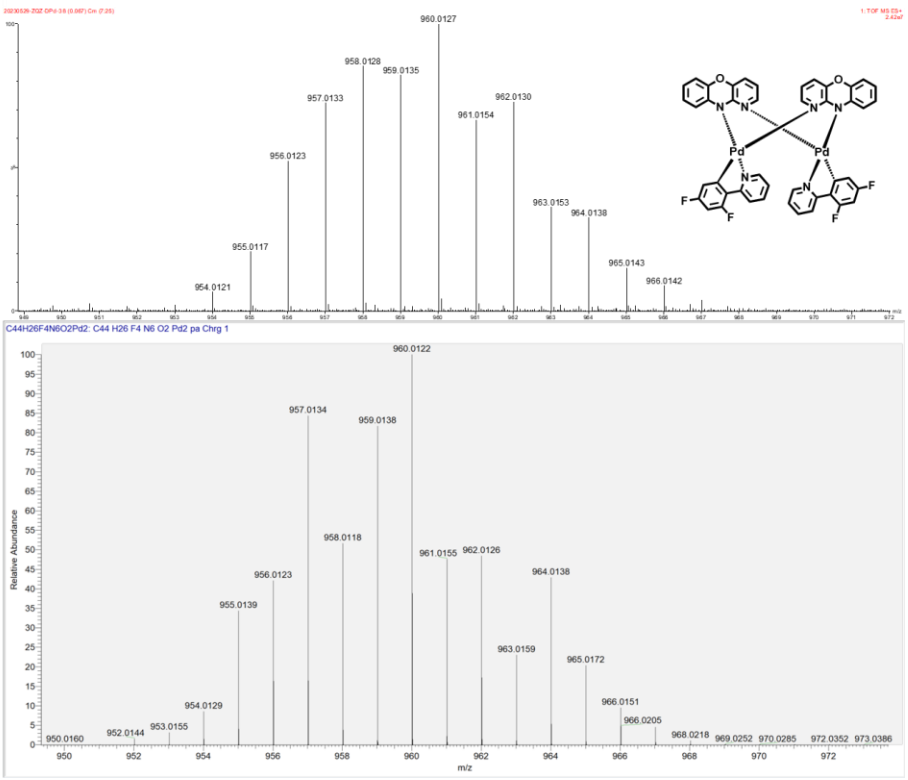

Figure S23. HR-MS spectrum of **1a**.

HRMS (EI+)
m/z found

HRMS (EI+)
m/z calculated

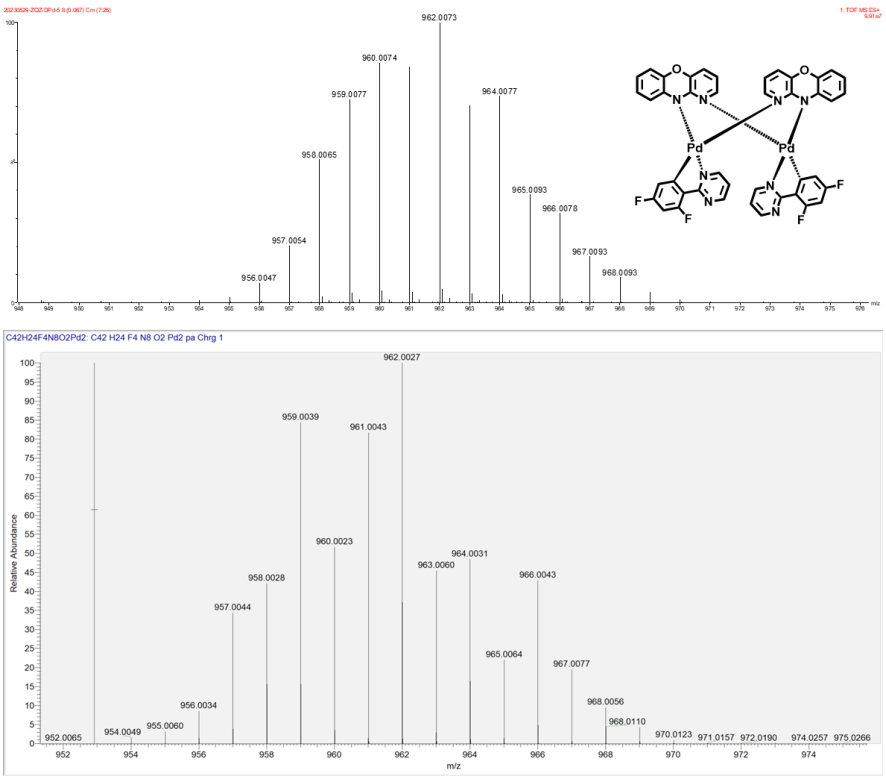

Figure S24. HR-MS spectrum of **2a**.

HRMS (EI+)
m/z found

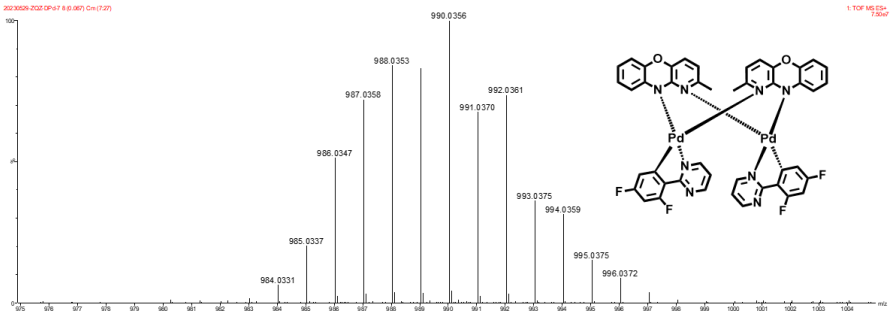

HRMS (EI+)
m/z calculated

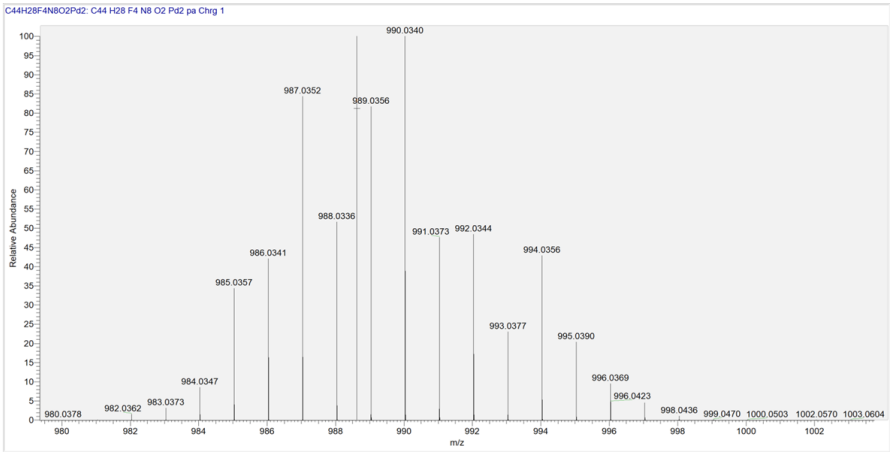

Figure S25. HR-MS spectrum of **2b**.